A Multi-Stage Home Energy Management System with Residential Photovoltaic Penetration

***Abstract*—Advances in bilateral communication technology foster the improvement and development of Home Energy Management System (HEMS). This paper proposes a new HEMS to optimally schedule home energy resources (HERs) in a high rooftop photovoltaic penetrated environment. The proposed HEMS includes three stages: *forecasting*, *day-ahead scheduling*, and *actual operation*. In the forecasting stage, short-term forecasting is performed to generate day-ahead forecasted photovoltaic solar power and home load profiles; in the day-ahead scheduling stage, a Peak-to-Average Ratio (PAR) constrained coordinated HER scheduling model is proposed to minimize the 1-day home operation cost; in the actual operation stage, a Model Predictive Control (MPC) based operational strategy is proposed to correct HER operations with the update of real-time information, so as to minimize the deviation of actual and day-ahead scheduled net-power consumption of the house. An adaptive thermal comfort model is applied in the proposed HEMS to provide decision-support on the scheduling of the heating, ventilating, and air conditioning (HVAC) system of the house. The proposed approach is then validated based on Australian real datasets.**

[1]***Index Terms*—Smart home, demand side management, demand response, energy management system**

NOMENCLATURE

[2]*Sets and Indices*

a, Φ	Index and set of the controllable appliances;
a', Φ^{ICA}	Index and set of ICAs;
a'', Φ^{NICA}	Index and set of NICAs;

Constants

Δt	Duration of scheduling time interval (hour);
T	Total number of scheduling time intervals;
γ	Cost coefficient of the RBESS depreciation;
$P^{bess,rate}$	Rated power capacity of the RBESS (kW);
$E^{bess,rate}$	Rated energy capacity of the RBESS (kWh);
P_a^{ca}	Rated power of controllable appliance a (kW);
$P_a^{ca,base}$	Base power of controllable appliance a (kW);
A	Area of the photovoltaic solar panel (m^2);
$C_{install}$	Photovoltaic source installation fee paid by the user ($);
N^{GY}	Number of guarantee year of the photovoltaic source;
σ	Photovoltaic Energy conversion efficiency;
P^{hvac}	Rated power of the HVAC (kW);
η^c, η^d	Charging loss (%) and discharging loss factors (%/month) of the RBESS;
η^l	Leakage loss factor (%/month) of the RBESS;
κ	Energy efficiency of the HVAC;
$pr(t)$	Electricity price at time t ($/kWh);
SOC^{min}	Lower SOC limit of the BESS;
$SOC^{\max}$	Upper SOC limit of the BESS;
$L(t)$	Forecasted total uncontrollable house load at time t (kW);
$P^{pv}(t)$	Forecasted photovoltaic solar power output at time t (kW);
$r(t)$	Forecasted solar radiation at time t (J/m^2);
d_i	Required operation duration of the ith AOA (hour);
χ	PAR threshold;
$\tau^{on}_{\min,i}, \tau^{off}_{\min,i}$	Minimum online and offline limits of ith ICA at t (hour);
t_a^{start}, t_a^{end}	Start and end time of the allowable operation time rage of the CA a;
ψ^{low}, ψ^{upp}	Lower and upper APMV limits;

Variables

$P^{bess}(t)$	Charging/discharging power of the RBESS at time t (kW);
$E^{bess}(t)$	Energy stored in the RBESS at time t (kWh);
$SOC(t)$	SOC of the RBESS at time t;
$s_a(t)$	Status of the CA a at time t: 0-OFF, 1-ON;
$\tau_i^{on}(t), \tau_i^{off}(t)$	Accumulated online and offline durations of ith IAOA at t under scenarios o and u (hour);
$L^{net}(t)$	Net load of the house at time t (kW);

I. INTRODUCTION

WITH the increasing penetration of information and communication technology (ICT) associated with distributed energy sources (e.g., renewable source, energy storage system, distributed generation unit), modern buildings are becoming complex micro cyber-physical systems. In these scenarios, expert systems are capable of enhancing the energy efficiency of buildings and, in particular, Home Energy Management Systems (HEMSs) have attracted in recent years significant attention in both academia and industry.

With the aim of providing decision-support for residential users, HEMSs often automatically schedule Home Energy Resources (HERs) to optimize energy consumption of houses/units. Different HEMSs can be developed for managing different kinds of HERs. Some HEMSs are developed to optimally schedule thermostatically controlled appliances (e.g., our previous works [1-3]). Some researches coordinately schedule various controllable household appliances together with the renewable energy sources and energy storage devices. For example, [4] proposed a scheduling model to optimally schedule the

operations of the household appliances under day-ahead forecasted real-time electricity pricings; [5] optimally scheduled a residential battery energy storage system (RBESS) and household appliances with solar power penetration; in [6], a load commitment framework was proposed to minimize the household operation costs. In [7], we proposed a multi-objective HEMS model by taking into account the renewable uncertainties. In [8], a HEMS was designed to dynamically schedule appliances in each dwelling unit, and based on which the power demand of the whole community was forecasted and reported to the utility. Our recent work introduced the service computing technology into smart home and proposed the concept of "demand side recommender system" [9-11], which can work in the manually operated home environment and recommend energy-aware products/suggestions to the homeowner. Most of aforementioned researches [1-8] focus on day-ahead scheduling of HERs. Only very limited works can be found addressing to gap between the forecasted and real-time data associated with the day-ahead and actual operation stages, respectively. Iwafune *et al*. [12] proposed a rule-based control strategy for actual operations of RBESS, by considering penetration of photovoltaic solar power.

The major contribution of this paper is to propose a multi-stage HEMS to coordinate day-ahead plan-making and actual operation. The proposed system significantly extends the work in [12] by considering the flexibility of controllable appliances and the heating, ventilating, and air conditioning (HVAC) system. In the forecasting stage, we employ an artificial neural network (ANN) based method for the day-ahead forecasting that relies on following three stochastic variables: solar radiation, ambient temperature, and must-run house load. Day-ahead forecasted data is then used as input to a proposed day-ahead HER scheduling model that accounts for the Peak-to-Average (PAR) ratio of the house consumption. In actual operation stage, a Model Predictive Control (MPC) based operation model is proposed to reduce the negative impact of the day-ahead forecasting error. Moreover, an Adaptive Thermal Comfort Model is introduced to provide decision-making support for the scheduling of HVAC. For clarity, the schematic overview of the proposed HEMS is summarized in Fig. 1.

This paper is organized as follows. Section II presents the models of HERs managed by the HEMS; Section III introduces the day-ahead forecasting method; Sections IV and V present the proposed day-ahead and actual HER operation models, respectively; the solution procedure is presented in Section VI; simulations are discussed in Section VII; and, finally, conclusion and future work are provided in Section VIII.

II. Home Energy Resource Models

A key step in the development of a HEMS is to establish suitable HER models and this section presents such models for a smart home environment.

A. Model of the Residential Battery Energy Storage System

Energy charging and the state-of-charge (SOC) of the RBESS is formulated as follows:

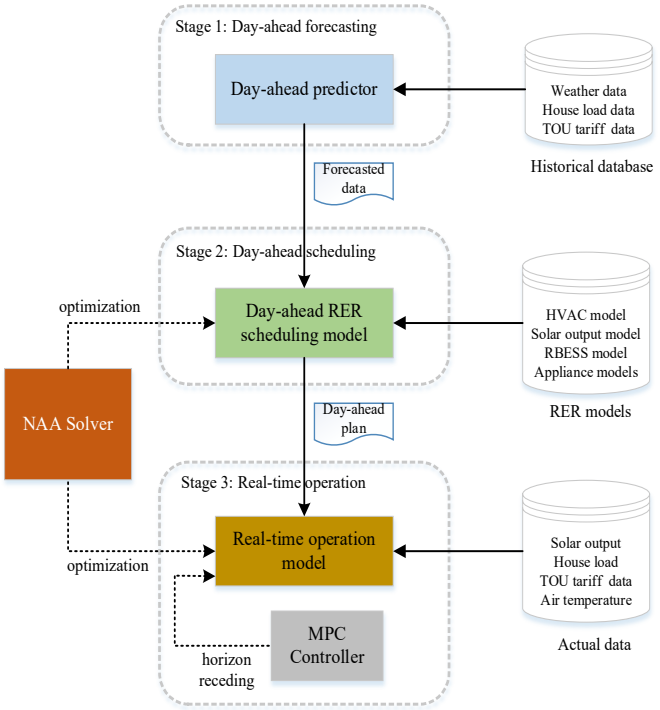

Fig. 1 Schematic of the multi-stage HEMS

$$E^{bess}(t+1) = E^{bess}(t) - \Delta t \cdot \eta^{d} \cdot P^{bess}(t) - \\ |P^{bess}(t)| \cdot \eta^{c} \cdot \Delta t - E^{bess}(t) \cdot \eta^{l} \cdot \Delta t \quad (1)$$

$$SOC(t) = E^{bess}(t) \Big/ E^{bess,rate} \quad (2)$$

where negative and positive values of $P^{bess}(t)$ indicate discharging and charging, respectively. Lifetime depreciation cost of the RBESS is calculated as follows:

$$C_{bess} = \gamma \cdot P^{bess}(t) \cdot \Delta t + \gamma \cdot E^{bess}(t) \cdot \eta^{l} \cdot \Delta t \quad (3)$$

B. Model of the Controllable Household Appliances

Controllable appliances can be subdivided in two classes: interruptible, controllable appliances (ICAs) and non-interruptible, controllable appliances (NICAs). ICAs refer to appliances whose operations can be interrupted and resumed later, such as clothes dryers and dish washers; NICAs refer to appliances whose operations are not allowed to be interrupted until they finish the work, e.g., coffee maker.

In this study, we assume the controllable appliances consume rated power (P_a^{ca}) when they are running, and consume zero power when they are turned off. For an ICA, it is assumed that it consumes a base power when it is interrupted. For example, a clothes dryer often includes a heating coil part and a motor part. When it is interrupted, the heating coil part stops working while the motor part continue running until the appliance is resumed. For convenience, we use $P_a^{ca,base}$ to denote the base power of appliance *a*. For NICA, the value of $P_a^{ca,base}$ is zero.

C. Model of Building Thermal Dynamics

An adequate modelling of the building thermal dynamics is essential for an efficient HVAC scheduling. In this study, we employ the third-order state-space thermal dynamics model

widely used in the literature [13], [14]. This model considers the impact of ambient temperature and solar irradiance on the indoor temperature, and is expressed as follows:

$$T_{j,t+1} = A \cdot T_{j,t} + B \cdot U_t \tag{4}$$

$$T_t^{in} = C \cdot T_t \tag{5}$$

where $T_t = [T_t^{in}, T_t^{im}, T_t^{om}]'$ is the state vector, in which T_t^{in} is the indoor temperature at time t (°C); T_t^{im} is the temperature of the thermal accumulating layer in the inner walls and floor of the building at time t (°C); T_t^{om} represents the temperature of the building envelop at time t (°C). $U_t = [T_t^{amb}, \Phi_t, \kappa \cdot P^{hvac}]'$ is the input control vector, where T_t^{amb} is the ambient temperature and Φ_t is the solar irradiation at time t (kW/m^2); and $C = [1, 0, 0]$. The building parameter matrices A and B can be calculated based on the inner walls and floor, and the thermal capacitances and resistances of the building.

D. Model of Human Indoor Thermal Comfort

Existing HVAC scheduling works [13], [15] restrict the indoor air temperature within a pre-specified comfort temperature band. However, in building environment science [16], people's thermal comfort is often evaluated through thermal comfort models, by taking into account the indoor temperature, humidity, clothing condition, etc. In previous work [2], [4], we integrated the ISO 7730 thermal comfort model into the direct load control of HVAC systems. ISO 7730 model is a PMV-PPD thermal comfort model (i.e. Predicted Mean Vote - Percentage People Dissatisfied) proposed by Fanger [16], and has been standardized by the American Society of Heating, Refrigerating and Air-Conditioning Engineers (ASHARE).

ISO 7730 model seeks to capture people's responses to the thermal environment in terms of the physics and physiology of heat transfer. It assumes the human body as a passive recipient of outdoor thermal stimuli, rather than an active one interacting with the person-environment system via multiple feedback loops. However, in real buildings, if changes occur that produce discomfort, people often react in various ways to restore their comfort (e.g., putting on/taking off clothing and taking in hot/cold drinks) [17]. Based on this realization, adaptive thermal comfort models have been developed, e.g. [17], to account for people's reactions. In this study, this adaptive thermal comfort model presented in [17] is employed to evaluate the user's indoor thermal comfort, which consequently affects the HVAC scheduling decisions. For a given indoor environment, the PMV value at time t ($PMV(t)$) is calculated following [18]:

$$PMV(t) = a \cdot T_{in}(t) + b \cdot P_v(t) - c \tag{6}$$

$$P_v(t) = rh(t) \cdot 10 \cdot e^{(16.6536 - 4030.183)/(T_{in}(t)+273)} \tag{7}$$

where $T_{in}(t)$ represents the indoor temperature at time t; $rh(t)$ and $P_v(t)$ represent the indoor relative humidity and vapor pressure in ambient air (mmHg), respectively; coefficients a, b, and c are determined by the user's clothing condition (I_{cl}), and can be found in [16]. Based on this, the adaptive PMV at time t ($APMV(t)$) is then calculated as:

$$APMV(t) = PMV(t) / (1 + \lambda \cdot PMV(t)) \tag{8}$$

where λ is the adaptive coefficient, representing effects of people's reactions. In this study, the value of λ is obtained from the Evaluation Standard for Indoor Thermal Environment in Civil Buildings of China [19], shown in table I.

E. Model of Photovoltaic Solar Power

Power output from photovoltaic solar panel is related to solar radiation and surface area and energy conversion efficiency of the panel, expressed as:

$$P^{pv}(t) = A \cdot \sigma \cdot r(t) \tag{9}$$

For a residential user, the daily discounted photovoltaic source investment cost is calculated by its installation fee paid by the user and the guarantee years provided by the utility:

$$C_{pv} = \frac{C_{install}}{N^{GY} \cdot 365} \tag{10}$$

III. Forecasting Methodology of Home Operation Environment

Due to the high volatility, residential load and solar power are difficult to be precisely forecasted, leading to non-ignorable risks associated with the decision making of home energy management. ANN has been widely used for forecasting of electricity load, solar power, electricity price, etc. (e.g. our previous work [20], [21]) because of its excellent nonlinear regression capability. Typical structure of a feed forward ANN is shown in Fig. 2. Given dataset $\{(\mathbf{x}_i, \mathbf{t}_i)\}_{i=1}^N$ with the inputs $\mathbf{x}_i \in \mathbf{R}^n$ and the outputs $\mathbf{t}_i \in \mathbf{R}^m$, the ANN with K hidden nodes and activation function $\phi(\cdot)$ for approximating N samples can be represented as:

$$f_K(\mathbf{x}_j) = \sum_{i=1}^{L} \beta_i \phi(\mathbf{a}_i \cdot \mathbf{x}_j + b_i), \quad j = 1, \ldots, N \tag{11}$$

TABLE I
Value Determination of Adaptive Coefficient (translated from [19])

Climate Zone of Building		Educational Buildings	Residential buildings, shops, hotels, and offices
Severe Cold Area	$PMV \geq 0$	0.21	0.24
	$PMV < 0$	-0.29	-0.5
Warm Area	$PMV \geq 0$	0.17	0.21
	$PMV < 0$	-0.28	-0.49

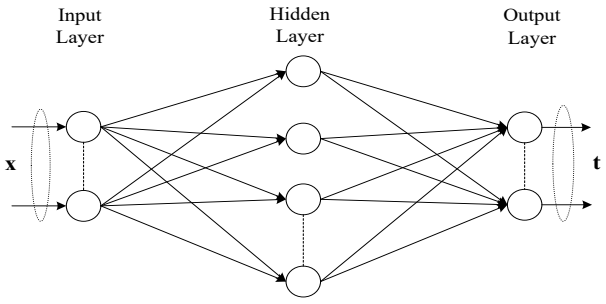

Fig. 2. The typical structure of artificial neural network.

where $\mathbf{a}_i$ represents the weight vector linking the i^{th} hidden node and the input nodes; β_i represents the weight vector linking the i^{th} hidden node and the output nodes; b_i represents the threshold of the i^{th} hidden node. Theoretically, parameters of NNs can be obtained by minimizing the following cost function:

$$C = \sum_{j=1}^{N}\left(\sum_{i=1}^{K}\beta_i\phi(\mathbf{a}_i\cdot\mathbf{x}_j + b_i) - \mathbf{t}_j\right)^2 \tag{12}$$

The bootstrap technique [22] is utilized to improve the regression accuracy. The inputs of the ANN based forecasting model vary with the forecasting target. For instance, for the day-ahead solar power forecasting, the inputs include numerical weather prediction, historical solar power, etc.

IV. Day-Ahead Scheduling Model of the Smart Home

Based on the forecasted profiles of solar radiation, air temperature, and house load, the day-ahead HER scheduling model is formulated to minimize the 1-day home operation cost:

$$\min F^{da} = C_{grid} + C_{pv} + C_{bess} \tag{13}$$

where C_{grid} represents the cost of purchasing power from the grid, which depends on the home net load and the TOU pricing; C_{pv} represents the discounted daily photovoltaic solar power generation cost; C_{bess} denotes the RBESS depreciation cost. C_{bess} and C_{pv} are calculated as Eqs. (3) and (10), respectively. C_{grid} is calculated as Eqs. (14):

$$C_{grid} = \sum_{t=1}^{T}\left[pr(t)\Delta t\cdot\max(L^{net}(t),0)\right] \tag{14}$$

in which:

$$L^{net}(t) = \sum_{a\in\Phi}s_a(t)P_a^{ca,*} + L(t) + P^{bess}(t) - P^{pv}(t) \tag{15}$$

$$P_a^{ca,*} = \begin{cases} P_a^{ca} & \text{if } s_a(t)==1 \\ P_a^{ca,base} & \text{if } s_a(t)==0 \end{cases} \tag{16}$$

Eqs. (14) and (15) represent the rated power and allowable SOC limit constraints; Eq. (16) ensures at the end of the day, the SOC of the RBESS must be larger than a pre-specified threshold (SOC^{desire}), so as to make it continuously serve the house in the incoming day.

Model (13) is subjected to following constraints:

(a) RBESS operational constraints.

$$\left|P^{bess}(t)\right| \le P^{bess,rate} \qquad \forall t = 1:T \tag{17}$$

$$SOC^{\min} \le SOC(t) \le SOC^{\max} \tag{18}$$

$$SOC(T) \ge SOC^{desire} \tag{19}$$

(b) Indoor thermal comfort constraint, which ensures the indoor thermal comfort must be kept within a comfort range.

$$\psi^{low} \le APMV(t) \le \psi^{upp} \qquad \forall t = 1:T \tag{20}$$

(c) CA operation time constraint specified by the homeowner:

$$s_a(t) = 0, \quad \forall a\in\Phi, t < t_a^{start}, t > t_a^{end} \tag{21}$$

(d) Operation cycle constraint that turns off the controllable appliance when the task is finished:

$$\sum_{t=1}^{T}(s_a(t)\cdot\Delta t) = d_a \quad \forall a\in\Phi \tag{22}$$

(e) NICA operation constraint that ensures no interruptions of the NISA until its work is completed:

$$\sum_{t=t_i^*}^{t_i^*+d_i/\Delta t} s_{a''}(t) = 1 \qquad \forall a''\in\Phi^{NICA} \tag{23}$$

where t_i^* represents the time interval when the ith NISA is first time to be turned on.

(f) ICA minimum online/offline time constraints. For interruptible SAs, the minimum online and offline time constraint is applied to protect their mechanical devices:

$$\begin{cases} \tau_{a'}^{on}(t) \ge \tau_{\min,i}^{on} & s_{a'}(t) == 0 \\ \tau_{a'}^{off}(t) \ge \tau_{\min,i}^{off} & s_{a'}(t) == 1 \end{cases} \qquad \forall a'\in\Phi^{ICA} \tag{24}$$

(g) PAR constraint. The PAR value of one-day operation of the house is maintained below a threshold:

$$\Gamma_{PAR} = \frac{\max_{t=1:T}\left|L^{net}(t)\right|}{\sum_{t=1}^{T}\left|L^{net}(t)\right|\Big/T} \le \chi \tag{25}$$

V. Actual Operation Model of the Smart Home

By solving the day-ahead scheduling model (13), the HEMS can estimate the one-day house net consumption profile and submit it to the load aggregator or utility [8], and the latter can make operation plans based on this forecasted load information. Therefore, the actual house net-load would be desired to follow the day-ahead schedule. Due to the inevitable forecasting error of the day-ahead stage, in the actual operation stage, the HEMS needs to update the HER operation decisions to follow the day-ahead schedule.

MPC [23] provides an effective solution to reduce the impact of forecasting errors by repeatedly updating the control decisions with the unfold of stochastic variables. MPC is not a specific control law, but is often defined as a control methodology characterized by following common steps:

(i) System modeling. The system model behaviors are predicted over a future horizon, called the predictive window;

(ii) Cost function definition. The closed-loop performance of the system model over the prediction window is specified;

(iii) Cost function optimization. The cost function is optimized as a function of the set of future control signals to be applied to the system model during the predictive window;

(iv) Receding horizon strategy. Only the control signal of the first (or first several) time interval is applied to the real process. In the next time step, the predictive window moves forward with one time interval, and all the algorithms repeat.

In this paper we propose a MPC based smart home actual operation strategy, depicted as Fig. 3. In each MPC round, stochastic variables of the home environment are forecasted over the predictive window, and a cost function is solved base on the day-ahead plan. Unlike the day-ahead forecasting, the forecasting in the MPC process occurs over a very short-term scale, and can thus be considered to be highly close to the actual value of stochastic variables. The cost function is defined to minimize the deviation of the actual and day-ahead forecasted net loads of the house:

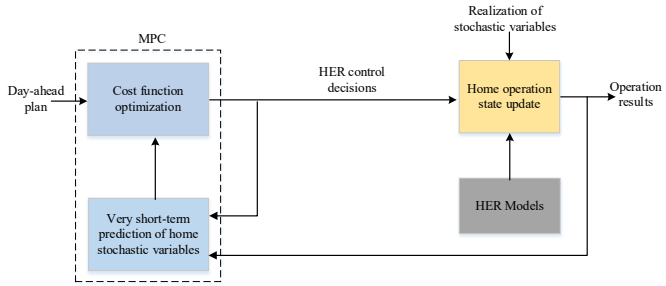

Fig. 3. Schematic of the MPC process

$$\min F^{act} = \sum_{t=t^{st}}^{t^{st}+T^{mpc}} \sqrt{\left(L^{net,act}(t) - L^{net}(t)\right)^2} \tag{26}$$

$$L^{net,act}(t) = \sum_{a\in\Phi} s_a^{act}(t) P_a^{ca,*} + L^{act}(t) + P^{bes,act}(t) - P^{pv,act}(t) \tag{27}$$

where $L^{net,act}(t)$ represents the net load of the house in the actual operation stage; t^{st} represents the starting time interval of the current MPC round; T^{mpc} is the predictive window size. The physical meanings of variables $L^{net,act}(t)$, $s_a^{rt}(t)$, $L^{act}(t)$, $P^{bes,act}(t)$, and $P^{pv,act}(t)$ are those already introduced for variables $L^{net}(t)$, $s_a(t)$, $L(t)$, $P^{bes}(t)$, and $P^{pv}(t)$ in Eq. (15) with the additional superscript '*act*' to denote that these new set of variables represent the actual values. The decision variables of model (26) include $s_a^{act}(t)$ and $P^{bess,act}(t)$, and all constraints (17)-(24) are applied. Since the actual operation objective is to make the actual home net-load follow the day-ahead schedule, constraint (25) is not applied in the actual operation model.

VI. Solving Approach

Models (13) and (26) are constrained, mixed-integer combinatorial optimization problems. Similarly to the unit commitment problem, their computational complexities over a finite optimization horizon are often NP hard. In the literature, heuristic algorithms are widely used to solve the HEMS model and obtain the global/near-global optimal solution in the high dimensional problem space [5], [6], [9]. In this paper, a new metaheuristic algorithm recently proposed by the authors, i.e., Natural Aggregation Algorithm (NAA) [24], [25], is employed to solve the proposed approach.

A. Brief Introduction of NAA

One nature of the group-living animals (e.g, fishes, insects, etc.) is that they often aggregate as multiple groups to take over resources (e.g., shelters, food, etc.). Such aggregation is beneficial for the swarm to share the resources, but the over-crowd of the group is disadvantageous for the swarm members. Biologists found the group-living animals have the intelligence to self-adaptively adjust the group sizes on multiple resource sites, to achieve the balance of the resource exploitation and exploration [26]. NAA essentially mimics the group-living animals' self-aggregation behaviors. It divides the whole population into multiple sub-populations, and uses a stochastic migration model to migrate the individuals among sub-populations. In each generation, local and global search strategies are applied to do the stochastic search in the problem space. More details of NAA can be found in [24]. NAA is designed to search for the global/near-global optimal solution in the high dimensional, nonlinear problem space. Such self-aggregation intelligence can well balance the exploitation and exploration in the searching process, which is an important consideration in the evolutionary computation domain. The experiment results in [24] also prove the superior performance of NAA on a range of benchmark nonlinear functions.

B. Workflow of NAA-Based Solving Approach

By applying NAA, in the day-ahead scheduling and actual operation models, each individual is encoded as a vector with $(|\Phi|+2)\cdot T$ and $(|\Phi|+2)\cdot T^{mpc}$ dimensions, respectively, representing a potential day-ahead plan and MPC decision scheme, respectively. Every $|\Phi|+2$ dimensions represent states of controllable appliances and HVAC (binary variables), and the charging/discharging power of the RBESS (continuous variables). The overall workflow of the HEMS is illustrated in Fig. 4. In the day-ahead forecasting stage, the values of stochastic variables are forecasted by the ANN and inputted into the day-ahead scheduling model. By applying NAA, the day-ahead scheduling decisions are generated, from which the house net-load profile is obtained. The house net-load profile is then included into the actual operation model, where the MPC scheduler uses NAA to solve the model and generates the actual control plan, based on the updated HER states and the realization of the stochastic variables.

VII. Simulation Study

Simulations are conducted to validate the proposed HEMS. All programs are implemented in Matlab and executed on a DELL PC with 128-G memory and two Intel Xeon processors.

A. Smart Home Environment Setup

The simulation is setup to describe a smart home environment in a typical summer working day. For this purpose, six controllable appliances are simulated: a pool pump (PP), dish washer (DW), rice cooker (RC), washing machine (WM), clothes dryer (CD), and vacuum robot (VR). The VR needs to be fully charged before a user-specified time point. Operations of the CD, VR charging, and PP are assumed to be interrupted, and those of the RC, WM, and DW are assumed to be non-interrupted. We obtain typical parameter values of the residential building from [13]. Table II shows the configuration of the home environment.

Day-ahead forecasting of solar radiation, outdoor air temperature, and house load are performed based on the 1-year solar radiation and air temperature data recorded in New South Wales (NSW, Australia), and residential load data published by the "Smart Grid, Smart City" project [27], respectively. The TOU tariff used in the simulations is reported by the Energy Australia [5], shown in table III. Installation fee and guarantee years of the rooftop photovoltaic solar panel are set to $6,220 and 25 years, respectively, according to the Australian residential solar business market survey [28]. The time interval is set to 15 minutes, and the scheduling period is assumed to be 24 hours, starting from 7am, when the homeowner starts his/her one-day life. For actual operation, the MPC window is set to be 4 hours, and the actual data of solar radiation, air temperature, and house load are applied.

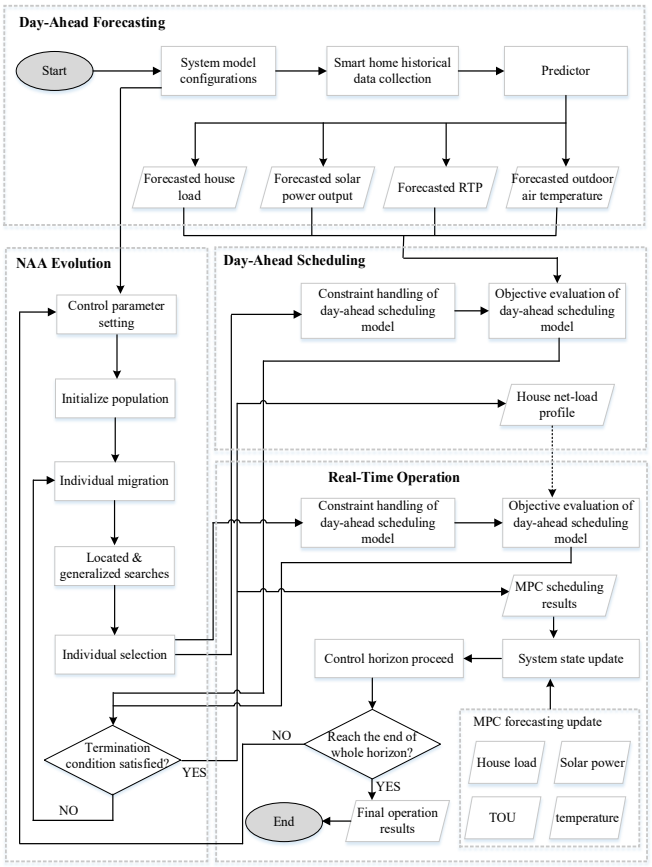

Fig. 4 Workflow of the HEMS

Control parameter settings of NAA are given in table IV. NAA includes six parameters [24] and these control, in groups of two, the individual migration, located search, and generalized search, respectively. For day-ahead scheduling, the time is relatively sufficient to accomplish the optimization (24-hour ahead), therefore N^{pop} and $G^{\max}$ are set as larger values, and the control parameters are set to encourage a wider global exploration; for the actual operation, the optimization needs to accomplish in one time interval (i.e., 15 minutes in this simulation), therefore N^{pop} and $G^{\max}$ are set as small values, and the control parameters are set to encourage the fast convergence [24].

B. Day-Ahead Forecasting Results

Figs. 5-7 show the real and forecasted profiles of the house load, solar power, and outdoor air temperature, respectively, produced by the ANN based forecasting method.

C. Day-Ahead RER Scheduling Results

Based on the forecasted information, the day-ahead scheduling is performed. Fig. 8 shows the final scheduled house net load profile. The electricity tariff is also plotted. It shows that the HERs are well scheduled to shift the peak house consumptions from the peak pricing to low pricing periods. The house net-load profile will be then used as the baseline for the actual operation.

Fig. 9 shows the day-ahead scheduled house consumption profile and the forecasted residential photovoltaic solar power profile. The house consumption is properly scheduled to show a desired shape and is consistent with the solar power distribution. In this manner, the house is scheduled to consume more power in the period with sufficient solar power (i.e., about 9am-3pm), and vice versa. This indicates the house is scheduled to be supplied by local energy sources, in which case the power purchase from the grid is significantly reduced.

TABLE II
CONFIGURATIONS OF THE SMART HOME ENVIRONMENT

Controllable Appliance Settings				
Name	OD	OTR	P_a^{ca}	$P_a^{ca,base}$
PP	4 hours	[9am, 6pm]	1.5 kW	0.1kW
DW	1.5 hours	[9am, 10pm]	2.4 kW	0.2kW
WM	1.5 hours	[11pm, 7am]	0.9 kW	0kW
RC	0.75 hour	[5pm, 7pm]	0.6 kW	0kW
CD	2 hours	[9am, 6:30pm]	2.5 kW	0.2kW
VR	2 hours	[9am, 6pm]	0.7kW	0.1kW
RBESS Settings				
Power Capacity		Energy Capacity	SOC^{desire}	
3kW		12kWh	30%	
SOC Lower Limit		SOC Upper Limit	γ	
10%		90%	0.1	
HVAC Settings				
Operation Time Range		ψ^{low}	ψ^{upp}	
[7-8:30am], [6-10pm]		-1	1	
Rated Power		κ	-	
3kW		2.5	-	
Homeowner's Clothing Settings				
Time Range	I_{cl}	Clothing Condition		
[7am, 10pm]	0.7	Short sleeve shirt, light trousers, shoes		
[10pm, 7am]	0.3	Underwear, T-shirt		

Note: 'OC' means 'operation duration; 'OTR' means 'operation time ranges'; clothing insulation value (I_{cl}) are obtained from [16].

TABLE III
ELECTRICITY TARIFF STRUCTURE

Time-of-Use	**Rate ($/kWh)**
Peak: 2pm-8pm	0.3564
Shoulder: 7am-2pm, 8pm-10pm	0.1408
Off-peak: 10pm-7am	0.0814
Critical Peak Price	**Rate ($/kWh)**
5pm-8pm	2.000

TABLE IV
CONTROL PARAMETER SETTINGS OF NAA

	Parameter Name	**Meaning**	**Day-Ahead Model**	**Real-Time Model**
Overall Control	N^{pop}	Population size	200	60
	$G^{\max}$	Maximum generation time	800	300
Sub-Population Control	N^S	Number of shelters	10	4
	Cp^S	Shelter capacity	20	15
Located Search Control	δ	Scaling factor	1	1
	Cr_{local}	Located crossover factor	0.6	0.8
Generalized Search Control	α	Movement Amplification	1.5	1.2
	Cr_{global}	Generalized crossover factor	0.3	0.1

D. Real-Time HER Scheduling Results

After the day-ahead scheduling, MPC is applied in the actual operation stage to update the control actions of HERs, so as to make the actual house net-load follow the day-ahead plan. We set the control window to be 3 hours (12 time intervals), and proceed the MPC process until end of the whole horizon is re-

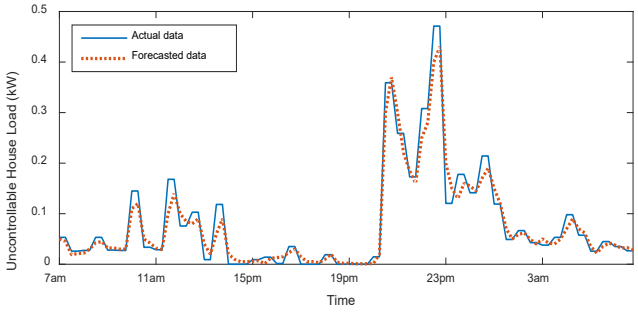

Fig. 5 Actual and forecasted house load

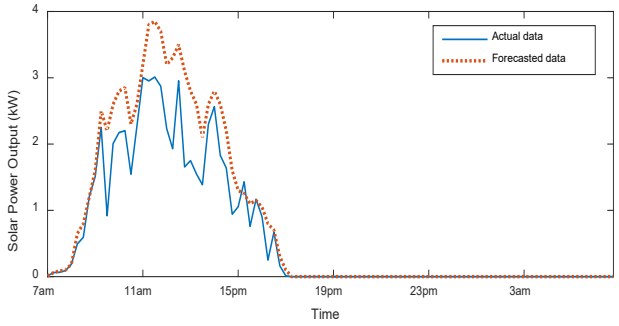

Fig. 6 Actual and forecasted solar power

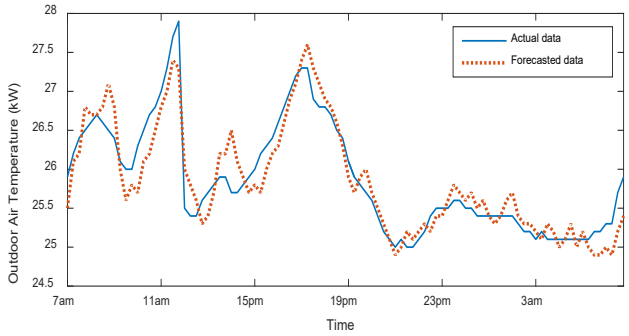

Fig. 7 Actual and forecasted air temperature

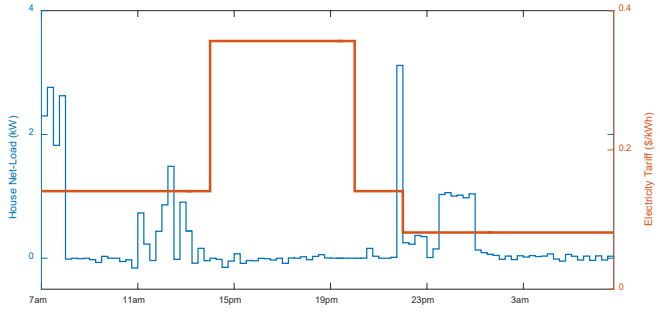

Fig. 8 Day-ahead scheduled house net-load profile

-ached. Fig. 10 shows the day-ahead and actual house net- load profiles. It can be seen that by applying MPC to on-line update the HER control decisions, the actual house net-load can generally follow the day-ahead plan, with only minor deviations. This result is compared with a base case, in which the day-ahead HER scheduling plan is strictly executed without any corrections. The result of the base case is shown in Fig. 10. It can be clearly seen that when there is no control action update for HERs, there is significantly larger deviations between the day-

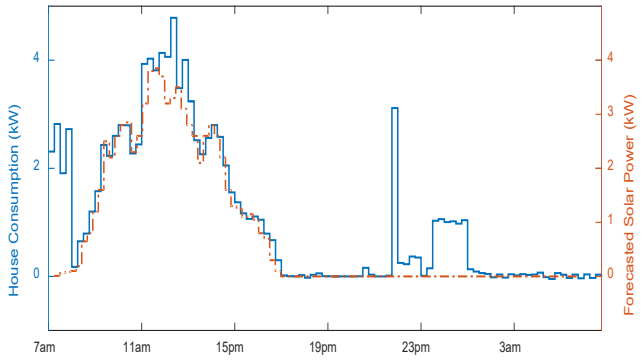

Fig. 9 Day-ahead scheduled house consumption and forecasted residential photovoltaic solar power output

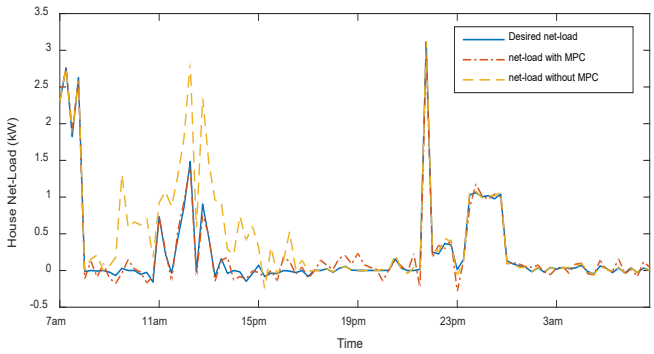

Fig. 10 Day-ahead and actual house net-load profiles

ahead and actual house net-load deviations, which are incurred by the forecasting errors.

Fig. 11 shows the HER scheduling decisions under day-ahead and real-time stages, respectively, with the MPC control window set as four hours. In actual operation stage, HER operation plans are updated with the realization of stochastic variables. The HVAC is controlled to maintain the indoor thermal comfort degree within the allowable range; the actual operation time ranges of controllable appliances are slightly different with the day-ahead plans, so as to minimize the day-ahead actual house net-loads. The actual operation of the RBESS shows a significantly larger deviation with the day-ahead plan, so as to compensate for the forecasting errors. Table V reports some numerical home operation results. It clearly shows that with MPC the actual operation results are much closer to the day-ahead plan than the results calculated for the case where day-ahead decisions are strictly executed without MPC corrections.

Fig. 12 shows the total deviation between the day-ahead plan and actual operation under different control window settings. With the increase of control window size, the deviation of day-ahead and actual operation is reduced. However, in practical situations, excessively large control windows would also yield unneglectable MPC forecasting errors. Therefore, the choice of control window depends on different implementation considerations.

The MPC based actual HER scheduling is further evaluated by comparing the following two scenarios: (1) by considering the solar power forecasting error, and (2) by assuming that there is no solar power forecasting error, i.e. representing the case of "perfect forecasting". The actual HER scheduling is executed under these two case scenarios with the same parameter setting

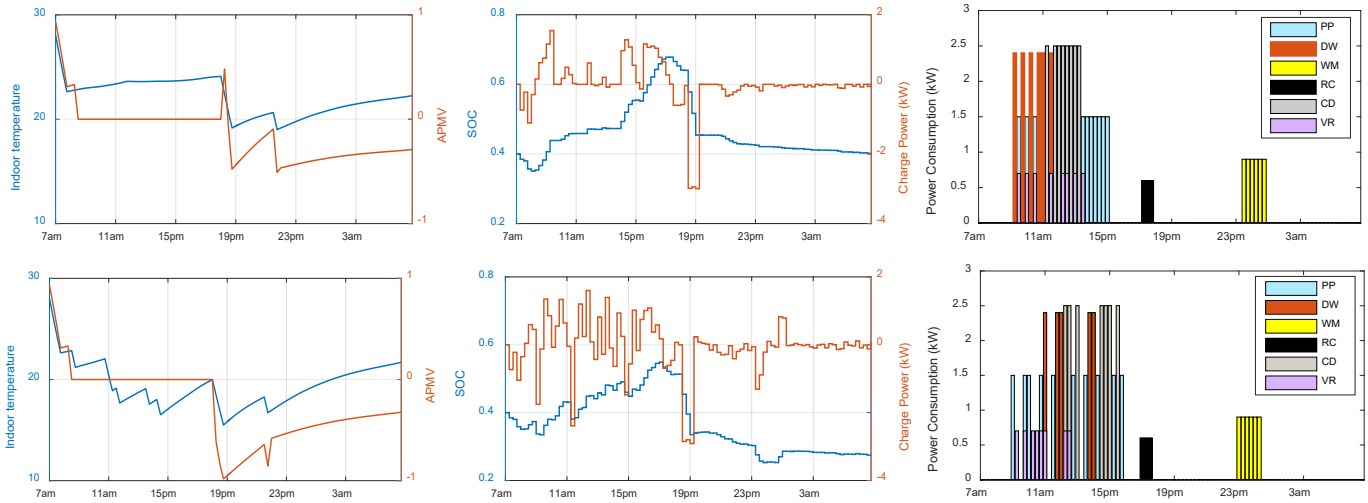

Fig. 11 HER operation decisions: (1) upper-left: indoor temperature and APMV profiles under day-ahead plan; (2) upper-middle: SOC and charging/discharging power of RBESS under day-ahead plan; (3) upper-right: CA operation time ranges under day-ahead plan; (4) lower-left: indoor temperature and APMV profiles under actual operation; (5) lower-middle: SOC and charging/discharging power of RBESS under actual operation; (3) lower-right: CA operation time ranges under actual operation;

TABLE V
Numerical Home Operation Results

Item	Day-Ahead Plan	Operation with MPC	Operation with-out MPC
Electricity Purchase Cost	$0.82	$0.97	$1.65
RBESS Operation Cost	$0.80	$1.15	$0.80
Discounted Daily Solar Generation Cost	$0.66	$0.66	$0.66
Total Cost	**$2.28**	**$2.78**	**$3.11**
Net-Load Deviation	**0.0**	**0.92kW**	**4.0kW**
PAR	0.11	0.09	0.07

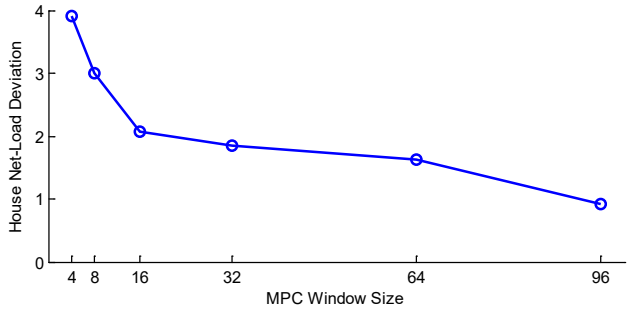

Fig. 12 Impact of the MPC control window size

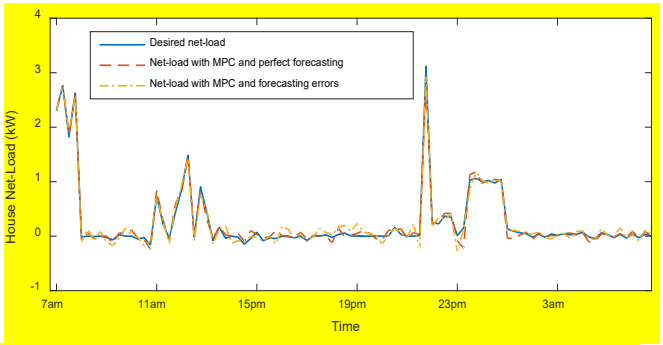

Fig. 13 House net-load profiles of MPC-based real-time operation with and without forecasting errors

introduced earlier. The scheduled net-load profiles are shown in Fig. 13. The total net-load deviation (calculated with Eq. (26)) for the MPC process with forecasting errors is 0.92 kW and this reduces to 0.79 kW for the "perfect forecasting" case. In the latter scenario, the final house net-load profile can better follow the desired house net-load profile generated by the day-ahead scheduling. However, even if there is no solar forecasting error, there are still some deviations (0.79kW in total) between the day-ahead scheduling and actual operation results. This is because the day-ahead scheduling performs a global optimization over the whole day period (24 hours), while the MPC process runs a local optimization that covers a limited horizon (4 hours in this simulation) in each round. The calculated results show that when considering the solar forecasting error, the total net-load deviation is only 0.13kW larger than the perfect forecasting case, indicating the satisfactory real-time correction capability of the MPC.

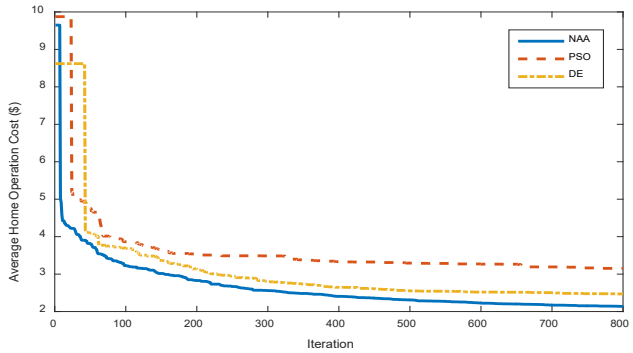

Fig. 14 Algorithm efficiency comparison

E. Algorithm Validation

The efficiency of NAA on the proposed HEMS is validated by comparing NAA with two commonly used heuristic optimization algorithm: Differential Evolution (DE) and Particle Swarm Optimization (PSO). The population size and maximum iteration time of the three algorithms are set to be the same with table IV. Control parameter values of DE and PSO are determined by several trials: For DE, F=0.8 and Cr=0.1; for PSO, w=0.8, C_p=1.5, C_g=1.5. For fair comparison purpose, five optimization trials are performed by each algorithm, and the average result is taken for comparison. Convergence curves of the three algorithms on solving model (13) is shown in Fig. 14. From Fig. 14, it can be seen that PSO performs worst, while DE

shows good search performance in the early iterations, but almost stops to improve the searching after around 600 iterations. NAA significantly outperforms PSO, and also shows stronger searching performance than DE during the whole iteration period. This observation is consistent with the experiments on benchmark functions reported in [24].

VIII. Conclusion and Future Work

This paper proposes a three-stage HEMS in a high photovoltaic penetrated home environment. In the first stage, ANN is applied to forecast the stochastic variables of the smart home; in the second stage, a day-ahead RER scheduling model is proposed to optimize the day-ahead plan while accounting for the PAR index; in the third stage, a MPC based actual operation model is proposed to update the control decisions based on the realization of the stochastic variables. With this approach, the APMV model is applied for the HVAC control, and the NAA algorithm is used to solve the proposed models. Simulations show that the proposed system can well coordinate the day-ahead and actual operations of the smart home.

The authors are currently developing stochastic programming based HEMS by considering the vehicle-to-home (V2H) technology and probabilistic characteristics of residential renewable energy.

References

[1] F. Luo, J. Zhao, etc., "Optimal dispatch of air conditioner loads in southern China region by direct load control," *IEEE Transactions on Smart Grid*, vol.7, no.1, pp.439-450, 2015.

[2] F. Luo, Z.Y. Dong, K. Meng, J. Wen, H. Wang, and J. Zhao, "An operational planning framework for large scale thermostatically controlled load dispatch," *IEEE Transactions on Industrial Informatics*, 2016.

[3] F. Luo, J. Zhao, H. Wang, X. Tong, Y. Chen, and Z.Y. Dong, "Direct load control with distributed imperialist competitive algorithm," *Journal of Modern Power Systems and Clean Energy*, vol. 2, pp. 385-395, 2014.

[4] Z. Zhao, W. Lee, Y. Shin, and K. Song, "An optimal power scheduling method for demand response in home energy management system," *IEEE Transactions on Smart Grid*, vol. 4, no. 3, pp. 1391-1400, 2013.

[5] M.A. Pedrasa, T. Spooner, and I. MacGill, "Coordinated scheduling of residential distributed energy resources to optimize smart home energy services," *IEEE Transactions on Smart Grid*, vol. 1, no. 2, 2010.

[6] F. Luo, Gianluca Ranzi, Gaoqi Liang, and Zhao Yang Dong, "Stochastic residential energy resource scheduling by multi-objective natural aggregation algorithm" *IEEE PES General Meeting*, 2017, accepted.

[7] Y. Ozturk, D. Senthilkumar, S. Kumar, and G. Lee, "An intelligent home energy management system to improve demand response," *IEEE Transactions on Smart Grid*, vol. 4, no. 2, pp. 694-701, 2013.

[8] F. Luo, G. Ranzi, X. Wang, and Z.Y. Dong, "Service recommendation in smart grid: vision, technologies, and applications," in *Proc. 9th International Conference on Service Science*, 2016.

[9] F. Luo, G. Ranzi, W. Kong, etc., "Non-intrusive energy saving appliance recommender system for smart grid residential users," *IET Generation, Transmission, and Distribution*, in press.

[10] F. Luo, G. Ranzi, X. Wang, and Z.Y. Dong, "Social information filtering based electricity retail plan recommender system for smart grid end users," *IEEE Transactions on Smart Grid*, 2017.

[11] F. Luo, Z.Y. Dong, K. Meng, J. Qiu, J. Yang, and K.P. Wong, "Short-term operational planning framework for virtual power plants with high renewable penetrations," *IET Renewable Power Generation,* 2016.

[12] Y. Iwafune, T. Ikegami, etc., "Cooperative home energy management using batteries for a photovoltaic system considering the diversity of households," *Energy Conversion and Management*, vol. 96, 2015.

[13] D. Nguyen and L.B. Le, "Joint optimization of electric vehicle and home energy scheduling considering user comfort preference," *IEEE Transactions on Smart Grid*, vol. 5, no. 1, pp. 188-199, Jan. 2014.

[14] A. Thavlov, "Dynamic optimization of power consumption," M.S. thesis, Tech. Univ. Denmark, Kongens Lyngby, Denmark, 2008.

[15] B. Ramanathan and V. Vittal, "A framework for evaluation of advanced direct load control with minimum disruption," *IEEE Trans. Power Syst.*, vol. 23, no. 4, pp. 1681-1688, Nov. 2008.

[16] ISO 7730:2005-Ergonomics of the thermal environment—Analytical determination and interpretation of thermal comfort using calculation of the PMV and PPD indices and local thermal comfort criteria [Online].

[17] R. Yao, etc, "A theoretical adaptive model of thermal comfort---adaptive predicted mean vote (aPMV)," *Building and Environment*, 2009.

[18] C. Buratti, P. Ricciardi, and M. Vergoni, "HVAC systems testing and check: A simplified model to predict thermal comfort conditions in moderate environments," *Applied Energy*, vol. 104, pp. 117-127, 2013.

[19] China Evaluation Standard for Indoor Thermal Environment in Civil Building [Online]. Available at: http://www.doc88.com/p-3824317544848.html

[20] C. Wan, Z. Xu, Y. L. Wang, Z.Y. Dong, and K.P. Wong, "A hybrid approach for probabilistic forecasting of electricity price," *IEEE Trans. Smart Grid*, vol. 5, no. 1, pp. 463-470, Jan. 2014.

[21] C. Wan, Y. Song, Z. Xu, G. Yang, A. Nielsen, "Probabilistic wind power forecasting with hybrid artificial neural networks," *Electric Power Components and Systems*, vol. 44, no.15, pp. 1656-1668, 2016.

[22] C. Wan, Z. Xu, P. Pinson, Z.Y. Dong, and K.P. Wong, "Probabilistic forecasting of wind power generation using extreme learning machine," *IEEE Trans. Power Systems*, vol.29, no.3, pp.1033-1044, May 2014.

[23] D.W. Clarke, Advances in Model Based Predictive Control, Oxford University Press, UK, 1994.

[24] F. Luo, J. Zhao, and Z.Y. Dong, "A new metaheuristic algorithm for real-parameter optimization: natural aggregation algorithm," in *Proc. IEEE Congress on Evolutionary Computation*, 2016.

[25] F. Luo, Z.Y. Dong, Y. Chen, etc., "Natural aggregation algorithm: a new efficient metaheuristic tool for power system optimizations," in *Proc. IEEE International Conference on SmartGridComm*, 2016.

[26] J. Ame, J. Halloy, C. Rivault, C. Detrain, and J. Deneubourg, "Collegial decision making based on social amplification leads to optimal group formation," *Proceedings of the National Academy of Sciences of the United States of America (PNAS)*, vol. 103, no. 15, pp. 5835-5840, 2006.

[27] Smart Grid, Smart City [Online]. Available at: http://www.industry.gov.au/ENERGY/PROGRAMMES/SMARTGRIDSMARTCITY/Pages/default.aspx.

[28] Australia Solar PV Power System Prices [Online]. Available at: http://www.solarchoice.net.au/blog/category/installation-advice/solar-system-prices-2/